International Journal of Computing and Digital Systems
ISSN (2210-142X)
Int. J. Com. Dig. Sys. 11, No.1 (Feb-2022)

http://dx.doi.org/10.12785/ijcds/110163

Classification of FHSS Signals in a Multi-Signal Environment by Artificial Neural Network

Muhammad Turyalai Khan[1], **Ahmad Zuri Sha'ameri**[1] **and Muhammad Mun'im Ahmad Zabidi**[1]

[1]*Division of Electronic and Computer Engineering, School of Electrical Engineering, Faculty of Engineering, Universiti Teknologi Malaysia, Johor Bahru, 81310, Johor, Malaysia*

Received 14 May 2021, Revised 14 Aug. 2021, Accepted 28 Jan. 2022, Published 15 Feb. 2022

Abstract: Frequency-hopping spread spectrum (FHSS) spreads the signal over a wide bandwidth where the carrier frequencies change rapidly according to a pseudorandom number making signal classification difficult. Classification becomes more complex with the presence of additive white Gaussian noise (AWGN) and interference due to background signals. In this paper, an artificial neural network (ANN) based system is proposed to classify FHSS signals in the presence of AWGN and background signal. The probability of correct classification (PCC) of the FHSS signals is computed by the linear discriminant (LD) and ANN. Based on the signal-to-noise ratio (SNR) range at 0.9 PCC, the performance of the LD and ANN respectively is 5.1 dB and 2.5 dB in the presence of AWGN only, whereas their performance is 14 dB and 2.3 dB when the background signal is present. Consequently, the ANN-based system outperformed the LD method by between 2.6 and 11.7 dB of SNR.

Keywords: Artificial neural network, Frequency-hopping spread spectrum, Linear discriminant

1. Introduction

Multi-signal environment contains different types of wireless technologies sharing a mutual frequency band [1]. An example would be Bluetooth, Wi-Fi, and Zigbee sharing the 2.4 GHz frequency [2]. The signals might have a constant or variable carrier frequency that depends on the wireless technology used. Utmost importantly, there must be no carrier frequency overlap amid the numerous wireless technologies, as this might cause interference among users. For example, two different Wi-Fi users can interfere with each other. Therefore, a spectrum monitoring system could be used to regulate carrier frequency usage across various wireless technologies as well as to detect unknown or unauthorized signal sources [3].

Frequency-hopping spread spectrum (FHSS) spreads the signal over a large bandwidth where the frequency is switched quickly in a pseudorandom manner that is known to the communicating parties for the synchronized communication [1], [4]. To switch the carrier frequency, the pseudo-noise (PN) pattern is utilized to produce the random number [5]. FHSS is employed in civilian as well as military applications such as drones [6], SINCGARS [7], and Bluetooth [8]. The military employs FHSS to evade jamming as well as interception by an opponent, whereas drones employ it to prevent interference from another drones by utilizing a hopping sequence [9]. The use of FHSS systems is allowed by the Federal Communications Commission (FCC) in unlicensed frequency bands which could be abused by a rogue device [10], for example, drones [6], [11]. Recent events that relate to drone abuse: (i) drones attacked an oilfield in Abqaiq, Saudi Arabia on Sep. 14, 2019 causing a 50% cut in oil production [12] and (ii) drone-assisted drug trafficking at Kranji, Singapore on Jun. 17, 2020 [13].

The analysis of an FHSS signal needs a technique appropriate for representing time-varying signal which is suitable for time-frequency (TF) analysis as it represents the time-varying signal mutually in both the domains of time and frequency [14]. Time-frequency distributions (TFDs) are divided into two categories: linear TFD and quadratic TFD (QTFD). The former like the short-time Fourier transform (STFT) [15] is utilized to acquire the time-frequency representation (TFR) of FHSS signals and estimate their parameters like hop duration as well as frequency. An issue pertaining to the TFR acquired from the STFT or spectrogram is the uncertainty principle that is the trade-off amid frequency and time resolution. To compare, the STFT has four times lower computational complexity (CC) than the QTFD [16]. Another category of the linear TFD is the wavelet transform that gives rise to the notion of multi-resolution analysis [17], it applies a variety of filters on a signal. It produces a low frequency resolution at the high frequency range of a signal, whereas a high frequency resolution at the low frequency range [18]. Because of this

E-mail address: turyalaikhan@graduate.utm.my, ahmadzuri@utm.my, munim@utm.my

attribute, it is inappropriate for the FHSS signals due to dispersion of the frequency content at the observed band of frequency. Generally, the QTFD produces high resolution in frequency and time, it applies if the cross-terms are attenuated but with high CC, whereas there is no cross-term in the STFT [14], [19]. The FHSS signal's parameters like hop frequency and duration could be measured utilizing the QTFD. For estimating these FHSS parameters, two approaches were utilized: the TF moments and instantaneous frequency [20]. Amid the two approaches, the latter precisely measure the parameters. The spectrogram method is utilized in this work due to low CC as this is significant for the applications of the FHSS to apply techniques in actual-time and on embedded systems.

After the estimation of a signal's parameters, it is followed by the classification task. The correlation among variables within data in the form of mathematical expressions is known as statistical modeling [21]. Statistical classifiers include: rule-based classifier [16], distance classifier using linear discriminant (LD) function [22], [23], [24], and maximum likelihood classifier [25]. In [24], FHSS signals classification is computed by the LD method that uses the Euclidean distance-based classifier. It has attained 90% probability of correct classification (PCC) at the SNR range of -1.6 to 3.5 dB in the existence of AWGN only, whereas its performance is declined to 0.9 to 12 dB with the existence of the background signal. Statistical models have less prediction ability and face difficulty to predict from noisy data. In comparison, machine learning (ML) has more predictive ability without human intervention since it can learn from data without depending on rule- based programming [21]. For example, the ML-based algorithm used for the classification of digital communication signals outperformed the maximum likelihood classifier by 12 dB of SNR at 90% accuracy [25], [26]. Examples of ML algorithms are decision trees, naive Bayes, and artificial neural network (ANN) [27]. Decision tree works by using a tree structure with a set of "if-then" rules for classifying data points which can easily overfit the data when the subbranches of the tree are overgrowing. Naive Bayes encodes probabilistic relationships among features by assuming every feature as independent which reduces the accuracy for overlapping classes. The ANN consists of a number of perceptrons to build a model like the human brain for decision making which can learn very complex functions and provides effective solutions in feature selection, and classification [27]. In some cases, large datasets are required for the ANN to be effective but it has powerful tuning options to prevent over- and under-fitting which makes it a good choice for achieving human-like decision making. The ANN is widely used for many pattern recognition applications such as speech signals [28], radar signals [29], and digital communication signals [26]. Classification of modulation recognition such as phase- shift keying (PSK), frequency-shift keying (FSK), and linear frequency modulation (LFM) is performed by using the STFT where 100% accuracy is achieved at 10 dB of SNR [30]. In [31], the ANN is used to classify PSK, FSK, and quadrature amplitude modulation (QAM) signals and achieved the PCC > 90% at SNR ≥ 0 dB. A supervised classification system based on TFD and multi-layer perceptron (MLP) is proposed to classify radar signals in which 98% of correct classification is achieved at 6 dB of SNR [29]. This method is improved in [32] by achieving 94.7% accuracy at -2 dB of SNR. Performance of the three classifiers such as radial basis function (RBF) neural network (NN), probability NN, and MLP NN is investigated in [26] for the classification of the amplitude shift-keying (ASK), PSK, and QAM signals. Among the three classifiers, the MLP NN performed best by achieving 95.7% accuracy at -2 dB of SNR. Despite its relatively higher CC, the ANN based on studied literature is used as a classifier in this paper due to its higher accuracy.

The uneven number of samples among classes in the training set degrades the performance of ML algorithms [33], [34]. The results achieved in [35] show the performance degradation of the classifier when trained on imbalanced data (original dataset). It is shown in [36] that the accuracy of the classifier is degraded by 5% on imbalanced data. Therefore, resampling is required on the minority classes to ensure a balanced number of samples among classes. Examples of resampling techniques are: random oversampling (ROS), random undersampling (RUS), synthetic minority oversampling technique (SMOTE), and majority weighted minority oversampling technique (MWMOTE) [37], [38], [39]. Among the simplest is the ROS in which minority samples are randomly duplicated to obtain a balanced dataset without introducing new information to the dataset. In the RUS, samples from the majority class are randomly removed which may cause the loss of important data. Synthetic samples from minority samples are created from SMOTE which increases the generalization ability of a classifier while the MWMOTE creates synthetic samples in specific regions.

The goal of this work is to develop an ANN-based system to achieve a precise classification of FHSS signals in the existence of AWGN and the background signal. Rapid switching of the carrier frequency according to a pseudorandom number makes the FHSS signals classification challenging. The ANN needs the training to classify various types of FHSS signals, which require a proper dataset. Hence, a dataset of the FHSS signals needs to be generated. A pseudorandom sequence of hopping frequencies observed from an FHSS signal represents one observation of all the possible hopping sequences of the signal. Therefore, a technique is developed that can derive the possible hopping sequences of the FHSS signal by using the hop frequencies. The uneven number of observations among classes in the training set degrades the performance of the ANN. The number of observations of an FHSS signal depends on the number of hop frequencies. Therefore, a given set of FHSS signals with a varying number of hop frequencies among the FHSS signals results in a different number of observations, thereby building an imbalanced dataset. Thus, resampling

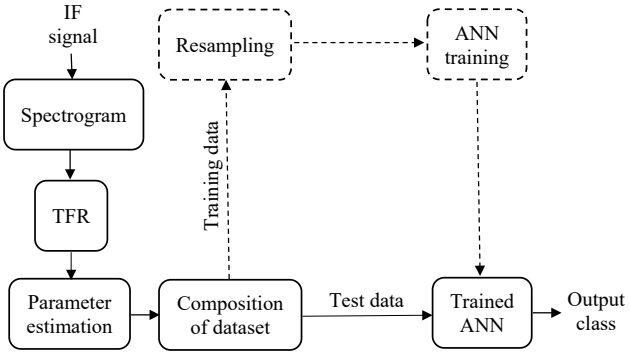

Figure 1. Block diagram of the proposed ANN-based classification system.

methods such as the ROS and SMOTE are performed to balance the dataset to enhance the ANN performance. From the studied literature, it is expected that the ANN with a balanced dataset will perform better compared to an imbalanced dataset.

The proposed ANN-based classification system shown in Fig. 1 is briefly described in this paragraph, whereas its detailed explanation is in Section 3. The spectrogram is produced from the intermediate frequency (IF) to acquire the TFR of the FHSS signal. From the TFR, the FHSS signal's parameters like hop frequency and duration are measured. Afterward, the dataset of the FHSS signals is derived followed by the segregation of the data into training and test data. Resampling is applied to the training data to ensure a balanced number of observations among the classes and used as input for the ANN training to obtain the trained ANN. The test data is used to evaluate the performance of the trained ANN.

The rest of the paper is structured as: the signal model and problem statement are defined in Section 2. The TFD, parameter estimation, and the proposed ANN-based system are described in Section 3. Section 4 presents the results and discussion, whereas the conclusions are summarized in Section 5.

2. Signal Model

In this section, the signals utilized in this work such as FHSS and orthogonal frequency-division multiplexing (OFDM) are defined. The FHSS-based wireless technologies like those utilized by Bluetooth and drones often use 2.4 GHz frequency band, which take a large bandwidth of 100 MHz [6], [40]. Hence, a radio-frequency (RF) signal with 2.4 GHz frequency is chosen, but this work could also be employed to another frequency bands, for example, 5.8 GHz. The Wi-Fi signal is represented by the OFDM signal, which will be treated as the background signal. For FHSS and OFDM, the modulation methods used in this work are binary phase-shift keying (BPSK) and quadrature phase-shift keying (QPSK), respectively. The expression for the FHSS signal is given as [41]:

$$s(t) = a(t)e^{j2\pi f_c(t)t}, 0 \le t \le T \tag{1}$$

where the signal is represented by $a(t)$, the signal duration by T, and the time-varying channel frequency by $f_c(t)$.

The OFDM signal that is often utilized in Wi-Fi is given as [42]:

$$v(t) = A\sum_{k=1}^{64} a(t)e^{j2\pi(f_c+f_k)t}, 0 \le t \le T \tag{2}$$

where the signal is represented by $a(t)$, the constant channel frequency by f_c, the subcarrier frequency by f_k, the frequency index by k which is in range of $1 \le k \le 64$, and the signal amplitude by A. Note that based on IEEE802.11 b/g/n standard, subcarrier spacing of $\Delta f_k = 312.5$ kHz with 64 subcarriers is used for Wi-Fi.

Realistically, noise corrupts the received signal, which is then interfered with by background signals that could be expressed as:

$$y(t) = s(t) + v(t) + n(t) \tag{3}$$

where the FHSS signal is represented by $s(t)$, the background signal by $v(t)$, and the additive white Gaussian noise (AWGN) by $n(t)$.

The FHSS signal with four cases of interference are evaluated for simulation motives as follows:

- Case 1: FHSS + AWGN
- Case 2: FHSS + AWGN + $1/\sqrt{2}$ OFDM
- Case 3: FHSS + AWGN + OFDM
- Case 4: FHSS + AWGN + $\sqrt{2}$ OFDM

The OFDM signal in Cases 2, 3, and 4 is incorporated within the range of the IF at 27 MHz frequency. In Case 2 and Case 4, multiplication by $1/\sqrt{2}$ and $\sqrt{2}$ forms the OFDM signal's power at half and double, respectively, with the FHSS signal's power.

A. Parameters of FHSS Signals

In this paper, a dataset of real signals is not used to verify the performance of the classifier. However, the parameters of the signals used are similar to FHSS signals used in [20], [43] and background signals such as OFDM signal [42]. Table I presents the parameters of the five FHSS signals, where each FHSS signal is dissimilar from others with respect to hop duration and hop frequencies. Amid the five FHSS signals, the FHSS_1 has the shortest hop duration that contributes in capturing 16 frequencies within

TABLE I. Parameters of the FHSS signals.

Signal	Hop Duration (μs)	No. of Hop Frequencies	Hop Frequencies (MHz)
FHSS_1	2	16	$f_c = k \times 6$ MHz; $k = 1, 2, \ldots, 16$
FHSS_2	3.5	9	$f_c = k \times 7$ MHz; $k = 1, 2, \ldots, 9$
FHSS_3	5	6	$f_c = k \times 15$ MHz; $k = 1, 2, \ldots, 6$
FHSS_4	6.5	4	$f_c = k \times 7$ MHz; $k = 1, 2, 3, 4$
FHSS_5	8	4	$f_c = k \times 15$ MHz; $k = 1, 2, 3, 4$

the signal length of 32 μs compared to the FHSS_2 that has less frequencies. Therefore, the hop frequency count relies on the hop duration and the length of the signal.

B. Parameters of OFDM Signal

The OFDM signal utilized in Wi-Fi, digital audio/video transmission, and 4G cellular technology is considered as a background signal in this paper. It depicts a Wi-Fi signal with a subcarrier spacing of 312.5 kHz, 64 subcarriers, and a channel bandwidth of 20 MHz. The OFDM signal's parameters employed in the paper are shown in Table II.

TABLE II. OFDM signal parameters.

Signal	Signal Length (μs)	No. of Subcarriers	Bandwidth (MHz)	Carrier Frequency (MHz)
OFDM	32	64	20	27

C. Problem Statement

An FHSS signal is a time-varying signal with a rapidly changing carrier frequency over time, as opposed to a fixed-frequency signal in which the frequency stays constant. The change in carrier frequencies across a large frequency range along with noise in the RF spectrum forms the FHSS signals classification difficult [41]. Furthermore, the sharing of frequency bands such as in the 2.4 GHz frequency band results in interference between the fixed frequency wireless technology (Wi-Fi) and FHSS based wireless technology (drone). Accurate classification of FHSS signals together with the necessity to scan a wide range of frequencies within a short time interval becomes a difficult challenge when combined with noise represented as AWGN, which is naturally present in wireless communication [6], [44].

ML is the analysis of algorithms that have the ability to automatically learn from observations of data [27]. An ML algorithm requires training for which a proper dataset is needed. A pseudorandom sequence of hopping frequencies observed from an FHSS signal represents one observation of all the possible hopping sequences of the signal. Therefore, a technique is required that can determine the total number of possible hopping sequences of the FHSS signal to determine the total number of observations in the dataset.

Most of the ML algorithms assume that the training set is evenly distributed among classes [33]. However, in many real-world applications, the number of observations among classes is often imbalanced which reduces the classification accuracy of an ML algorithm [34]. The number of observations of an FHSS signal depends on the number of hop frequencies. Therefore, a given set of FHSS signals with a varying number of hop frequencies among the FHSS signals results in a different number of observations, thereby building an imbalanced dataset. Thus, a method is required to balance the dataset for the increased learning and decision-making capacity of an ML algorithm.

3. Analysis and Classification of FHSS Signals

The method employed for the classification of FHSS signals in the existence of AWGN and the background signal is described in this section. TFD is used to analyze the FHSS signals followed by the parameter estimation, determination of the dataset, and the network structure of the employed ANN. The dataset generation and experiments simulation were performed in MATLAB.

A. Time-Frequency Distribution

The signal is down converted from RF at 2.4 GHz to the IF at 50 MHz. The shift in the frequency from RF to IF is shown in Fig. 2.

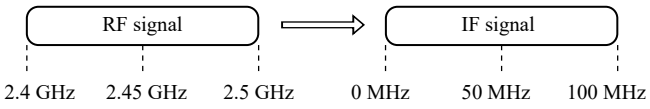

Figure 2. Time-frequency analysis bandwidth.

The TFR can be obtained from the IF using the spectrogram that is expressed as follows [14]:

$$X(n,k) = \sum_{m=0}^{N-1} x(m)w(m-n)e^{-j2\pi km/N_w} \quad (4)$$

$$S_x(n,k) = |X(n,k)|^2 \quad (5)$$

where the signal length is represented by N, the signal by $x(n)$, the window function by $w(n)$ with length N_w, and the TFR by $S_x(n,k)$.

A value of the threshold is required to distinguish the FHSS signals from background signals defined in Section 2. The determination of the threshold is obtained from a baseline signal, which is without the presence of FHSS signals, but could contain any combination of the background signals or at least AWGN. From the start, the baseline signal will be obtained and its power spectrum would be acquired by frequency marginal of TFR [14], [20].

$$P_x(k) = \sum_{n=0}^{\infty} S_x(n,k) \quad (6)$$

The peak value of AWGN's power spectrum is used as a default threshold P_{T_def}, because it is present throughout the frequency range. For background signals such as OFDM, it appears at a certain range of frequency and has peak power greater than AWGN. For the OFDM signal's frequency, a larger threshold is required, which can be expressed as:

$$P_T(k) = max(P_{T\_def}, P_B(k)) \tag{7}$$

where the threshold at k frequency is represented by $P_T(k)$ and the maximum power of a background signal by $P_B(k)$.

The threshold setting $P_T(k)$ over the spectrum is shown Fig. 3, where it is customized adaptively to its peak value. For this example, the chosen values of the threshold for specific bands of frequency are:

(a) 0.001 W for 0 – 28 MHz, 45 – 75 MHz, and 93 – 100 MHz.

(b) 0.004 W for 28 – 45 MHz.

(c) 0.002 W for 75 – 93 MHz.

B. Parameter Estimation

In this section, the FHSS signal's parameters like the hop duration and hop frequency will be measured from the TFR [43].

1) Hop Frequency Estimation

The power spectrum is obtained from the TFR by using (6) to estimate hop frequencies from the peaks of the power spectrum as shown in Fig. 4. The expression for the measured hop frequency and signal bandwidth for BPSK can be formulated as:

$$\hat{f_c} = f_p \tag{8}$$

$$\hat{f_{BW}} = f_{upp} - f_{low} \tag{9}$$

where f_p is the peak frequency, f_{low} and f_{upp} are the lower and upper frequencies estimated from 50% peak power.

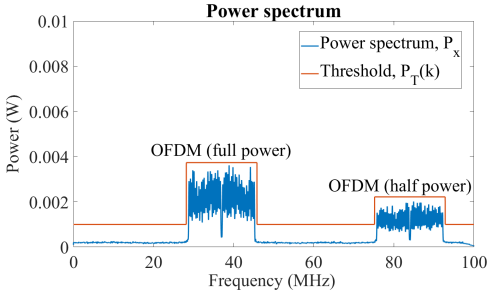

Figure 3. Threshold setting from power spectrum of baseline signal.

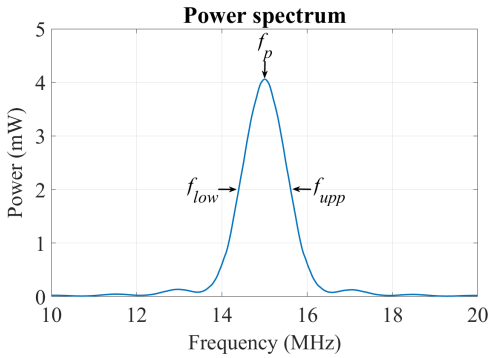

Figure 4. Power spectrum from TFR.

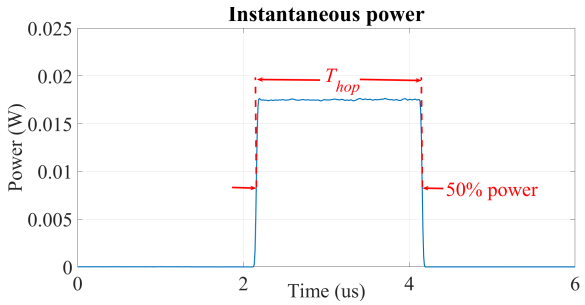

Figure 5. Instantaneous power from TFR.

2) Hop Duration Estimation

The TFR is assessed within a range of frequency close to the hop frequency to determine the hop duration at that frequency and the instantaneous power is given as:

$$P_i(n) = \sum_{k=f_{low}}^{f_{upp}} S_x(n,k) \tag{10}$$

where f_{low} and f_{upp} are the lower and upper frequency limit, respectively, within the hop frequency measured in (8). By estimating the pulse width at a reference level of 50% from the peak as illustrated in Fig. 5, the instantaneous power at each measured hop frequency is computed and utilised to measure the hop duration.

C. Composition of Dataset

A dataset is required to train the ANN that will be used to classify the various types of FHSS signals. Ideally, the dataset size must be sufficiently large as well as balanced to optimize the classification performance [27]. The following is the derivation of the FHSS signals dataset.

1) Determination of Number of Possible Hopping Sequences of FHSS Signals

A pseudorandom sequence of hopping frequencies observed from an FHSS signal represents one observation of all the possible hopping sequences of the signal. The following example describes the derivation of the total number of possible hopping sequences of an FHSS signal.

An FHSS signal with three hop frequencies (f_1, f_2, f_3) is selected in this example. For the given hopping sequence, only one frequency should appear at any given hop duration. By considering all observations, the possible hopping sequences for this signal are shown in Table III where each column represents a hopping sequence of the frequencies. There are six possible hopping sequences of three frequencies which can be expressed as 3! = 6. Thus, it can be concluded that the factorial of the number of hop frequencies of an FHSS signal produces the possible hopping sequences.

TABLE III. Possible hopping sequences for an FHSS signal with three hop frequencies.

Hopping Sequence 1	Hopping Sequence 2	Hopping Sequence 3	Hopping Sequence 4	Hopping Sequence 5	Hopping Sequence 6
f_1	f_1	f_2	f_2	f_3	f_3
f_2	f_3	f_1	f_3	f_1	f_2
f_3	f_2	f_3	f_1	f_2	f_1

For a particular type of FHSS signal, all the possible hopping sequences can be calculated as follows:

$$P_{hs} = n! \tag{11}$$

where P_{hs} is the possible hopping sequences and n is the number of hop frequencies of an FHSS signal.

Based on the signal parameters defined for all the FHSS signals in Table I, all the number of possible hopping sequences for each signal is calculated by (11) using the number of hop frequencies. The results for all FHSS signals are shown in Table IV. It is observed that the number of possible hopping sequences of an FHSS signal increases with the number of hop frequencies. Between the FHSS signals, FHSS_1 and FHSS_2 have more possible hopping sequences compared to the rest of FHSS signals.

2) Determination of Number of Selected Hopping Sequences of FHSS Signals

Once the number of possible hopping sequences is determined for all FHSS signals using (11), the next step is to calculate the number of selected hopping sequences that will be used to determine the dataset. It is not practical to use all the possible hopping sequences, especially for FHSS_1 and FHSS_2 due to their large numbers that contribute to time complexity and computation cost [45]. Thus, it is important to find a suitable number of selected hopping sequences to make inferences from the possible hopping sequences.

TABLE IV. The number of possible hopping sequences for all FHSS signals.

Signal	No. of Hop Frequencies	No. of Possible Hopping Sequences
FHSS_1	16	2.09×10^{13}
FHSS_2	9	362880
FHSS_3	6	720
FHSS_4	4	24
FHSS_5	4	24

A similar problem is also encountered in social sciences where it is required to infer the characteristics of a population based on data collected from samples from the population because it is not practical to gather data from the entire population due to the difficulty of getting the cooperation to participate in the study. Furthermore, the risk of irrelevant intervention can occur if more samples are used than required. The following equation can be utilized to determine the sample size from a population [46].

$$s = \frac{X^2 NP(1-P)}{d^2(N-1) + X^2(1-P)} \tag{12}$$

where s is the required sample size, X^2 is the chi-square value for 1 degree of freedom at desired confidence level which is 3.841, N is the population size, P is the population proportion (assumed to be 0.5 as this will provide maximum sample size) and d is the degree of accuracy expressed as a proportion which is 0.05. In our work, the population size and the required sample size are considered as the number of possible hopping sequences and the number of selected hopping sequences, respectively. Thus, the number of selected hopping sequences for the FHSS signal can be calculated by using (12).

From this equation, the number of selected hopping sequences for FHSS_1 is:

$$s = \frac{3.841(2.09 \times 10^{13})(0.5)(1-0.5)}{(0.05)^2(2.09 \times 10^{13} - 1) + 3.841(1-0.5)} \approx 384$$

where $N = 2.09 \times 10^{13}$ for the FHSS_1 as determined in Table IV, s is the number of selected hopping sequences for FHSS_1, values for X^2, P and d^2 are discussed in the previous paragraph. Similarly, the numbers of selected hopping sequences according to (12) for the FHSS_2, FHSS_3, FHSS_4, and FHSS_5 are 384, 250, 23, and 23 respectively. Therefore, the number of selected hopping sequences among the FHSS signals used in this study is imbalanced.

D. Structure of Dataset

In this subsection, the derivation of the FHSS signals dataset is discussed. It is followed by segregating the dataset into training and testing sets. The main objective in this subsection is to determine the total number of observations from the number of selected hopping sequences in the dataset for all the FHSS signals. The structure of the dataset

TABLE V. Dataset of the FHSS signals and noise.

Class	No. of Selected Hopping Sequences	SNR (dB) Levels	Total No. of Observations	Training Observations	Testing Observations
FHSS_1	384	4, 6, 8, 10, 12, 14	384 × 6 = 2304	1620	684
FHSS_2	384	4, 6, 8, 10, 12, 14	384 × 6 = 2304	1620	684
FHSS_3	250	4, 6, 8, 10, 12, 14	250 × 6 = 1500	1050	450
FHSS_4	23	4, 6, 8, 10, 12, 14	23 × 6 = 138	96	42
FHSS_5	23	4, 6, 8, 10, 12, 14	23 × 6 = 138	96	42
Noise			2304	1620	684
Total			8688	6102	2586

of the FHSS signals and noise is shown in Table V where noise is included as a separate class in the dataset due to the possibility of no signal at the ANN input. Thus, the ANN has to be intelligent enough to differentiate between noise and FHSS signals. Following is the derivation of the dataset: first, the number of selected hopping sequences is determined in previous sub-section, then the dataset is generated under six SNR levels from 4 dB to 14 dB of SNR with step size of 2 dB for the ANN training [47]. The latter is chosen to cover the range from low to high SNR within the operating condition of the ANN. Each SNR level will contain the number of selected hopping sequences, so multiplying six to the number of selected hopping sequences of each class produces the total number of observations of each class. For noise, the number of observations selected is equal to the number of the majority class (FHSS_1 or FHSS_2) observations. Thus, the total number of observations in the dataset is 8688.

Splitting of a dataset into two parts that is training and testing takes place in supervised learning where it is a common practice that the training-set contains 70 to 80 percent of data while the remaining data is used for testing [27]. Therefore, in this work, 6102 observations (70%) are used for the ANN training and 2586 observations (30%) are used for testing as shown in Table V.

The dataset structure in Table V is imbalanced because of the different number of hop frequencies among the FHSS signals that result in different numbers of observations. A significant decline of area under the receiver operating characteristic curve (AUC) is observed in [35] when the ANN is trained on imbalanced data. The increase of class imbalance in the training-set has a progressively detrimental effect on ANN's performance. To handle the imbalanced dataset, resampling is required to balance the dataset which will be discussed further in the following subsection.

E. Classification of FHSS Signals

The LD and the ANN-based methods are proposed to classify FHSS signals in the existence of AWGN as well as the background signal. The following are the detailed explanations of these methods.

1) Linear Discriminant

LD is a function that is a linear combination of the components of feature vector **x** [48].

$$g(x) = \mathbf{w}^T\mathbf{x} + w_0 \tag{13}$$

where weight vector is represented by **w**, a feature vector by **x**, and the bias by w_0. To estimate distance between patterns, the Euclidean distance could be utilized, which is used to make recognition choices [22]. It is given as:

$$d(x, y) = \sqrt{\sum_{i=1}^{l} |x_i - y_i|^2} \tag{14}$$

where **x** and **y** represent the two vectors or points and l represents the elements in each vector.

The pseudo code of the LD method for the classification of the five FHSS signals is shown in Algorithm 1.

Algorithm 1: Linear Discriminant (LD)

Data: Ideal FHSS signals x_i where $i = 1, 2, \cdots, 5$;
Estimated FHSS signal y.
Result: Classified signal z.
Determine the Euclidean distances amid the ideal and estimated FHSS signals: $\mathbf{d}$ = [norm $(y - x_i)$];
Find the minimum distance amid the determined Euclidean distances: $m = min(\mathbf{d})$;
if m = *first point of* d **then**
  z = FHSS_1
else if m = *second point of* $\boldsymbol{d}$ **then**
  z = FHSS_2
else if m = *third point of* $\boldsymbol{d}$ **then**
  z = FHSS_3
else if m = *fourth point of* $\boldsymbol{d}$ **then**
  z = FHSS_4
else if m = *fifth point of* $\boldsymbol{d}$ **then**
  z = FHSS_5
else z = unknown;

2) Artificial Neural Network

The ANN pattern recognition is used as a classifier which uses the scaled conjugate backpropagation algorithm [49] for the training with tan-sigmoid activation function at the hidden layer and SoftMax at the output layer. Tan-sigmoid provides fast convergence of training algorithms

while SoftMax determines the multi-class probability at once [48]. ANNs are static networks in which the architecture should be pre-determined to fit the problem and it is fixed. The architecture of employed ANN for the classification of the FHSS signals is shown in Fig. 6 where the input layer is composed of 32 nodes (each receiving one input from the feature vector), the output layer has six elements (five elements indicate the predicted FHSS signals and one element indicate the noise only) and there is one hidden layer comprising of 32 neurons. There are five different FHSS signals which have a varying number of hop frequencies and durations, thereby having a different number of elements of each signal. Therefore, zero-padding is needed to get a fixed-length input vector [50]. Zero-padding is applied to all the FHSS signals except FHSS_1 because FHSS_1 has 32 elements (16 hop frequencies and 16 hop durations) which are equal to the input layer of ANN while all the other FHSS signals have less than 32 elements.

3) Resampling Methods for Imbalanced Dataset

The following are the resampling methods used in this paper.

a) Random Oversampling

ROS works by randomly duplicating the minority class observations until the class distribution is balanced [37]. The structure of the training data becomes balanced after applying the ROS on minority classes (FHSS_3, FHSS_4, FHSS_5). Hence, the total number of training observations becomes 9720, as there are six classes where each class will equally have 1620 observations of training.

b) Synthetic Minority Oversampling Technique

SMOTE creates synthetic observations by randomly selecting a minority observation and then compute its k-nearest neighbors by using (14) among minority observations [38]. The synthetic observation is generated as:

$$S = [(M_2 - M_1) \times r] + M_1 \tag{15}$$

where M_1 is a randomly selected minority observation, M_2 is the nearest neighbour, r is a uniformly distributed random number between 0 and 1 and S is the newly generated synthetic observation. The training data becomes balanced, the same as described in the previous paragraph.

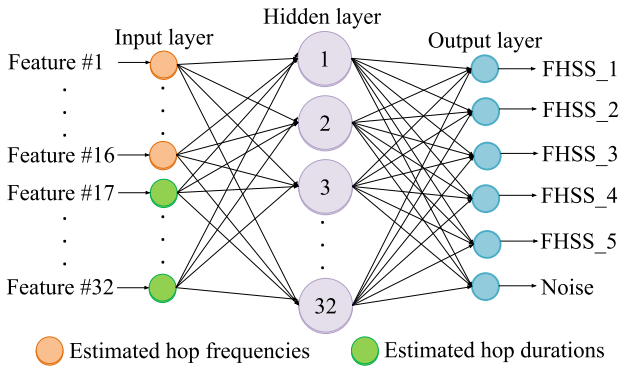

Figure 6. The ANN architecture employed for the classification of the FHSS signals.

F. k-Fold Cross-Validation

In k-fold cross-validation (CV), data are split into k-folds of equal size where $k-1$ folds are used for training and the remaining fold is used for validation as shown in Fig. 7 [51]. This process repeats k-times and then the classifier is evaluated on the test data. Validation is used to measure the performance of a network, and to halt training when the performance stops improving to avoid overfitting. 5-fold CV is used in this paper due to the large dataset.

4. Results

This section discusses and illustrates the TFR of the FHSS signals with the background signal. Thereafter, the PCC of the FHSS signals is computed for various SNR levels for all four cases stated in Section 2. The training of the proposed model of ANN is conducted three times. Therefore, the total number of methods conducted for each case is four: (i) LD, (ii) ANN with imbalanced data (ANN-ID), (iii) ANN-ROS, and (iv) ANN-SMOTE. Thereafter, the SNR range at 0.9 PCC of FHSS signals for all the four cases is evaluated. Finally, the training performance of ANN with respect to cross-entropy error is discussed.

A. Time-Frequency Representation

The TFR of the FHSS signals in the existence of AWGN and the background signal is shown in Fig. 8. A fixed frequency Wi-Fi signal included within the range of the IF at 27 MHz frequency is used as the background signal. The the FHSS_5 has the longest hop duration, whereas the FHSS_1 has the shortest hop duration, thereby contributing in 16 and 4 hop frequencies, respectively, inside the signal length of 32 μs.

B. Probability of Correct Classification

1) Case 1: FHSS + AWGN

The plots of PCC versus SNR where interference is modeled as AWGN are shown in Fig. 9. In all four methods of Case 1, the FHSS_4 signal with the fewer hop frequencies performs best, whereas the FHSS_1 signal with

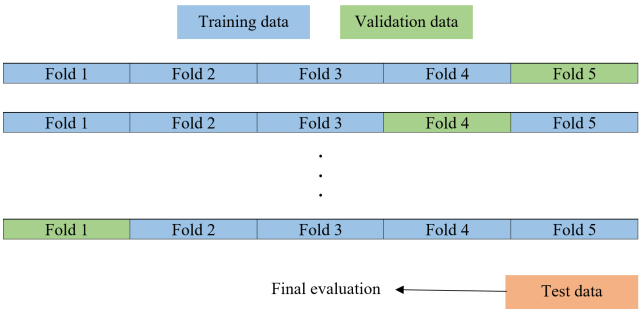

Figure 7. Block diagram of the 5-fold CV [48].

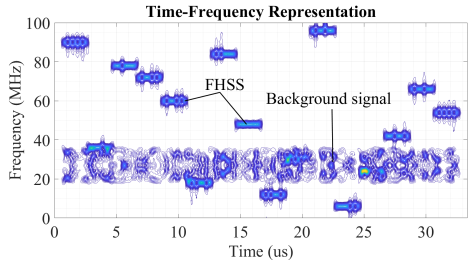

(a) FHSS_1

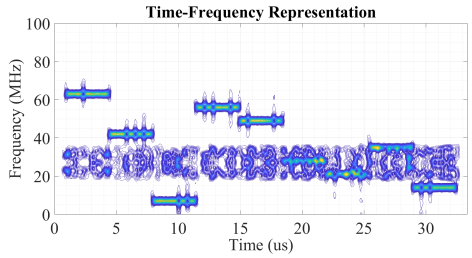

(b) FHSS_2

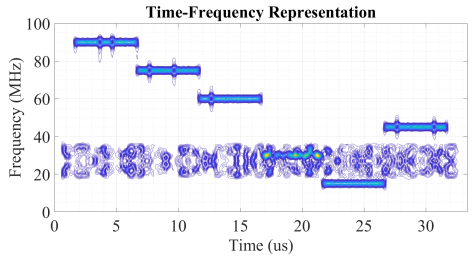

(c) FHSS_3

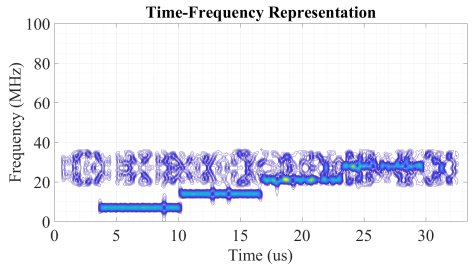

(d) FHSS_4

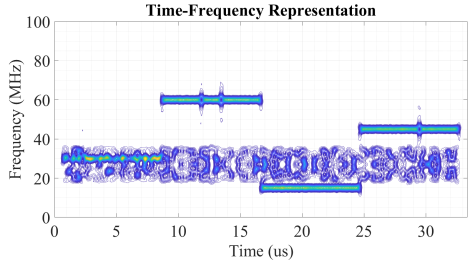

(e) FHSS_5

Figure 8. TFR of the FHSS signals in the presence of AWGN and the background signal.

the greater hop frequencies performs worst. Between the FHSS_4 and FHSS_5, the FHSS_5 performs less due to the class overlap [34] with the FHSS_3 and FHSS_1.

2) Case 2: FHSS + AWGN + 1/√2 OFDM

In this case, interference is modeled as AWGN, with the OFDM signal acting as the background signal, where the power of the latter is half that of the FHSS signal. The performance of the LD is declined significantly due to the background signal while the ANN still performs well as shown in Fig. 10. For all the methods of Case 2, FHSS_2 performs least because its three frequencies are overlapping with the background signal as depicted in Fig. 8(b) while the rest of the FHSS signals have lesser overlapping frequencies.

3) Case 3: FHSS + AWGN + OFDM

In this case, the OFDM signal's power is equivalent to the FHSS signal's power. The LD method's performance is negatively affected by an increase in the power of the background signal, but it does not have much effect on the ANN as shown in Fig. 11.

4) Case 4: FHSS + AWGN + √2 OFDM

The FHSS signal's power is half with the OFDM signal's power in this case. The overall performance is almost the same as in Case 3, an increase in the power of the background signal has negative affect on the performance of the LD method, but it has not much effect on the ANN as shown in Fig. 12.

C. Box Plots of SNR Range at 0.9 Probability of Correct Classification

Box plot is a visual representation of statistical data based on the five-number summary: minimum, first quartile, median, third quartile, and maximum [52]. The prompt appearance of the center, spread, and overall range make the box plot ideal for comparing distributions. In this section, the results achieved in the previous subsection are summarized by using the box plots as shown in Fig. 13. The distribution of the FHSS signals within the ranges shown in the box plots at 0.9 PCC are as follows: FHSS_3, FHSS_4, and FHSS_5 signals with least number of frequencies are close to the minimum SNR limit while FHSS_1 and FHSS_2 signals with the most number of frequencies are close to the maximum SNR limit. Based on the SNR range, the best performance is for Case 1 and the worst performance is for Case 4. This is expected in Case 4 since the interference is not just AWGN but also background signal due to OFDM. Furthermore, the power of the FHSS signal halves the background signal power. The performance for Case 2 and Case 3 where the background signal is present but at lower or equal power to the background signal produced better performance than Case 4.

It is observed from Case 1 that the narrowest and the widest SNR ranges (SNR range: difference between maximum and minimum SNR limit) among the ANN based methods are 2.4 dB and 2.5 dB which are smaller compared

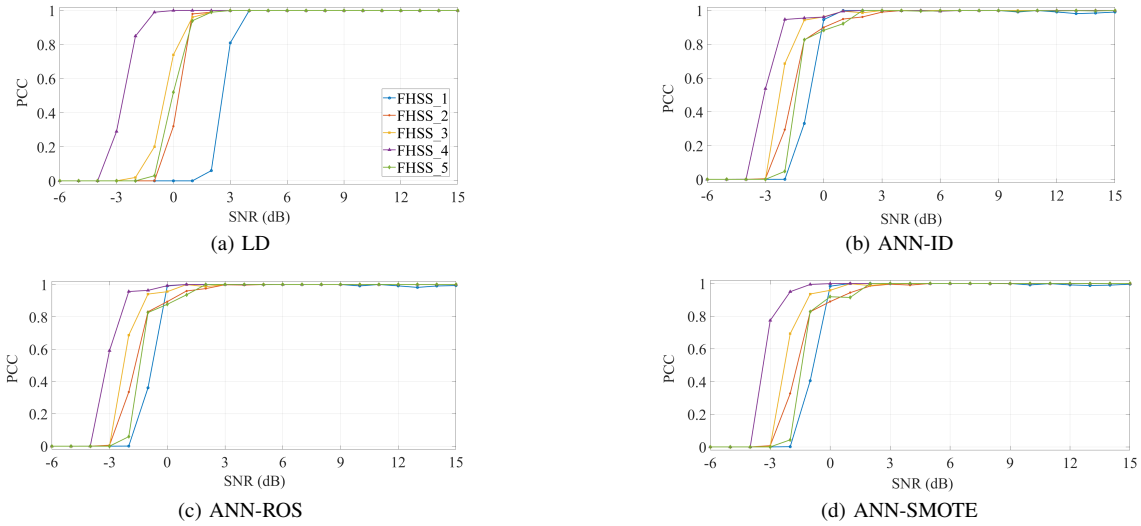

(a) LD (b) ANN-ID

(c) ANN-ROS (d) ANN-SMOTE

Figure 9. PCC of the FHSS signals for Case 1: FHSS + AWGN.

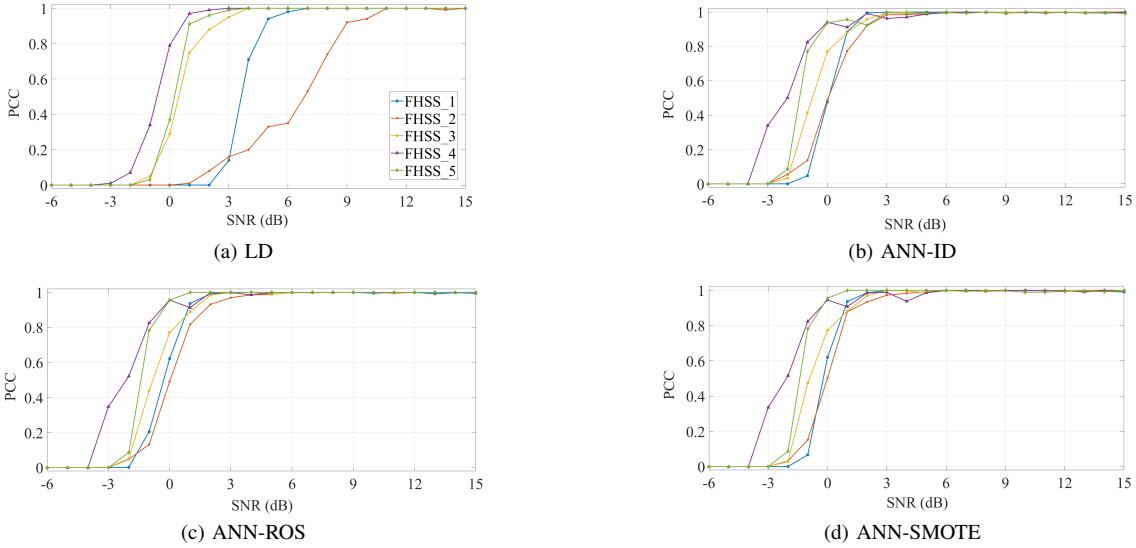

(a) LD (b) ANN-ID

(c) ANN-ROS (d) ANN-SMOTE

Figure 10. PCC of the FHSS signals for Case 2: FHSS + AWGN + $1/\sqrt{2}$ OFDM.

to the SNR range of 5.1 dB of the LD method. Similarly, in Case 4, the SNR ranges among the ANN based methods are 1.7 dB and 2.3 dB which are smaller compared to the SNR range of 14 dB of the LD method. These results indicate the more consistent and better performance of the ANN based methods than the performance of the LD. Furthermore, in Case 4, the SNR ranges for the ANN-SMOTE and ANN-ROS are 1.7 dB and 1.9 dB which are less than the SNR range of 2.3 dB of the ANN-ID.

The ANN-SMOTE performed better than the ANN-ROS in all the four cases. This is because the SMOTE adds artificial observations to the training dataset which increases the generalization ability of the ANN while the ROS does not introduce any new information to the training dataset. Thus, it can be concluded that: (i) The proposed ANN based system performed consistently well in both Case 1 and Case 4 while the performance of the LD is inconsistent and degraded significantly in Case 4. (ii) The ANN performed better with the balanced dataset than with the imbalanced dataset. Furthermore, Table VI shows the comparison of the average classification accuracy at 0 dB of SNR of the ANN-SMOTE with related works. The classification performance of the ANN-SMOTE is better than [24], [29], and [31], whereas close to [26].

D. Cross Entropy Error of Artificial Neural Network

In this section, the cross-entropy (CE) error of the training of the proposed ANN model conducted three times is discussed. CE is the measure of error between computed

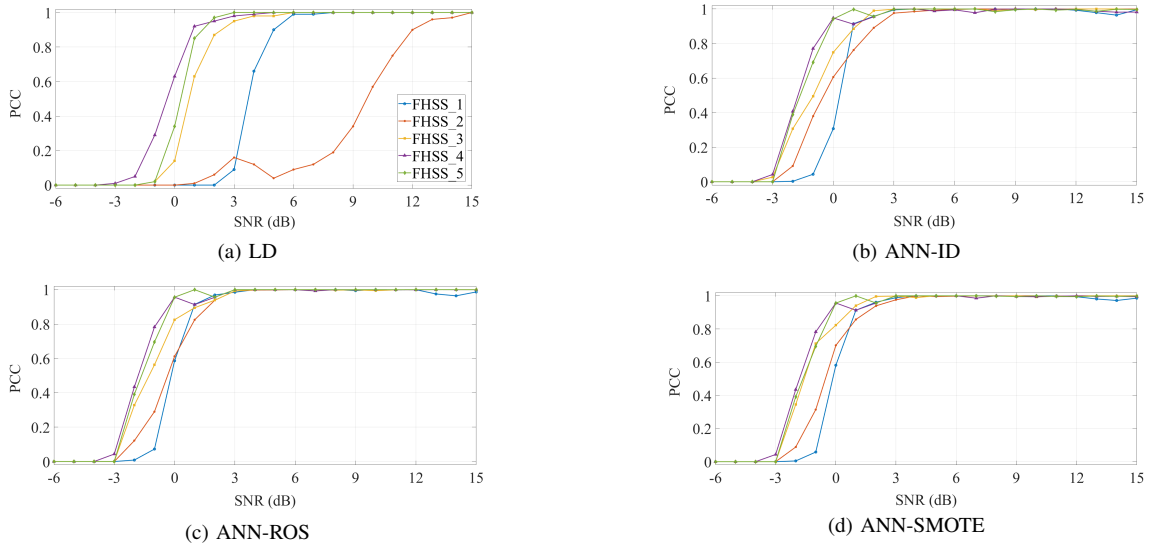

(a) LD (b) ANN-ID

(c) ANN-ROS (d) ANN-SMOTE

Figure 11. PCC of the FHSS signals for Case 3: FHSS + AWGN + OFDM.

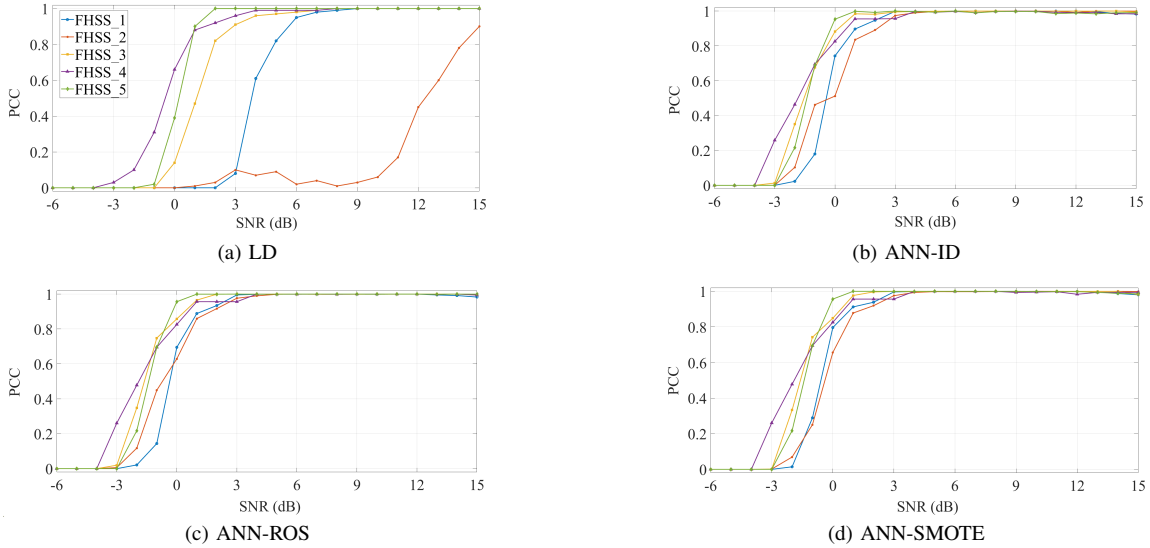

(a) LD (b) ANN-ID

(c) ANN-ROS (d) ANN-SMOTE

Figure 12. PCC of the FHSS signals for Case 4: FHSS + AWGN + $\sqrt{2}$ OFDM.

TABLE VI. Comparison of classification performance with related works.

Method	Signal Type	Average Accuracy at SNR = 0 dB
ANN [31]	Modulated signals	90%
MLP [29]	Radar signals	82%
MLP [26]	Modulated signals	99.51%
LD [24]	FHSS signals	51%
ANN-SMOTE	FHSS signals	95.77% (Case 1)

or predicted outputs and target outputs of the training data [53]. Minimizing CE error results in good classification, lower values are better, and zero CE means no error.

Fig. 14 shows the learning performances of ANN training for three methods with respect to CE. In Fig. 14(a), the ANN-ID model achieved the best validation performance of 0.0017 CE error at the epoch of 43 which means that the model is optimized at the epoch of 43. Although the training curve is converging after the epoch of 43, the performance of the model no longer continues to improve, as the CE error for validation starts increasing which may indicate the possibility of overfitting. Therefore, to avoid overfitting, early stopping of training is applied if the error increases

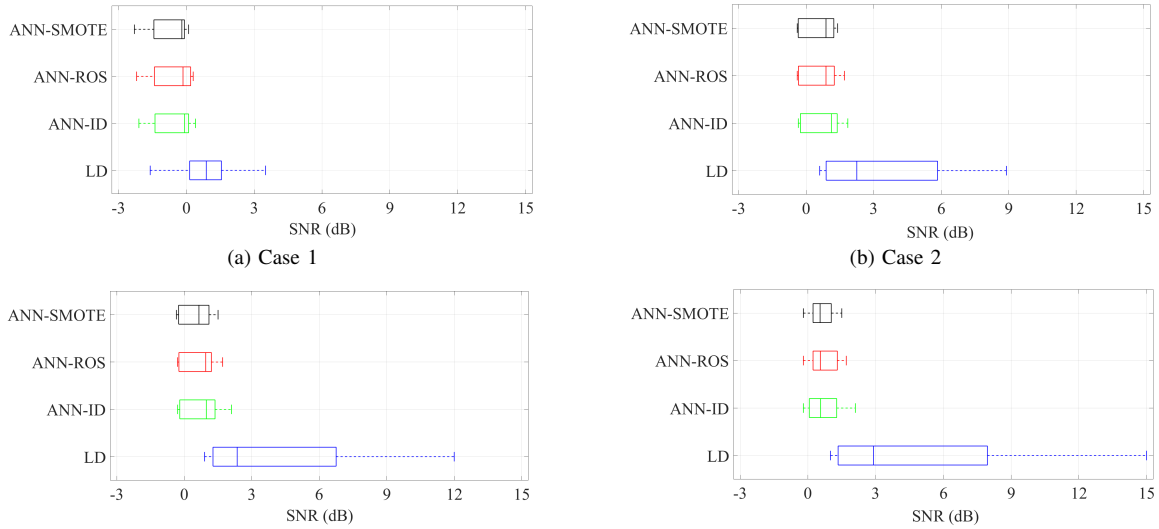

(a) Case 1 (b) Case 2

(c) Case 3 (b) Case 4

Figure 13. Box plots of SNR range at 0.9 PCC: (a) Case 1: FHSS + AWGN, (b) Case 2: FHSS + AWGN + $1/\sqrt{2}$ OFDM, (c) Case 3: FHSS + AWGN + OFDM, and (d) Case 4: FHSS + AWGN + $\sqrt{2}$ OFDM.

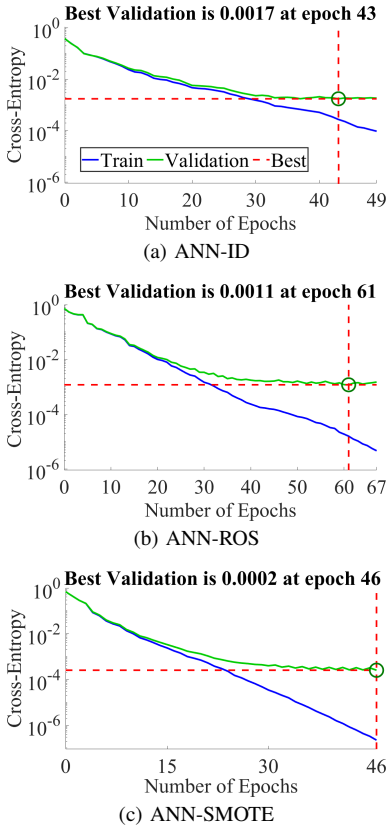

(a) ANN-ID

(b) ANN-ROS

(c) ANN-SMOTE

Figure 14. CE error of the ANN.

for six consecutive epochs [54]. In Fig. 14(b), the ANN-ROS model achieved the best validation performance of 0.0011 CE error at the epoch of 61 which is slightly less than the ANN-ID but it took 18 more epochs to converge to minimum CE error compared to the ANN-ID. So, the ANN-ROS model converges slower than the ANN-ID. In Fig. 14(c), the ANN-SMOTE model achieved the best validation performance of 0.00025 CE error at the epoch of 46 which is less than the other two ANN models.

Furthermore, the validation curve converges until the last training epoch as shown in Fig. 14(c). The performance of ANN-SMOTE continues to improve until the training curve reaches its goal of CE error below 10^{-6}. This increases the generalization ability of ANN that is why the ANN-SMOTE model performs better than the other two models of ANN.

5. Conclusion

The use of an ANN-based system was proposed to classify FHSS signals in the existence of AWGN and the background signal. In this approach, from the TFR, the FHSS signal's parameters like hop frequency and hop duration were measured. The ANN requires training for which a proper dataset is needed. Therefore, a technique was developed to derive the total number of possible hopping sequences of an FHSS signal that were used to determine the total number of observations in the dataset. Due to a varying number of hop frequencies among the FHSS signals, the issue of an imbalanced dataset occurred that degraded the performance of the ANN. Therefore, to enhance the ANN's performance, resampling methods such as the ROS and SMOTE were used to balance the dataset.

The PCC of the FHSS signals for various SNR levels was evaluated. Based on the SNR range at 0.9 PCC in the

worst case of interference (Case 4), the SNR ranges of the LD, ANN-ID, ANN-ROS, and ANN-SMOTE are as follows: 14 dB, 2.3 dB, 1.9 dB, and 1.7 dB, respectively. These results show that the ANN-SMOTE method outclassed the LD method by 12.3 dB (the difference between the SNR ranges: 14 dB – 1.7 dB) of SNR. Furthermore, the ANN-SMOTE performed better by 0.6 dB of SNR than the ANN-ID.

Acknowledgment

The authors would like to thank Universiti Teknologi Malaysia (UTM) for providing the resources for this research.

References

[1] J. G. Proakis and M. Salehi, *Digital communications*. McGraw-Hill, 2001.

[2] E. Fernández de Gorostiza, J. Berzosa, J. Mabe, and R. Cortiñas, "A method for dynamically selecting the best frequency hopping technique in industrial wireless sensor network applications," *Sensors*, vol. 18, no. 2, p. 657, 2018.

[3] A. Boyacı, A. R. Ekti, S. Yarkan, and M. A. Aydın, "Monitoring, surveillance, and management of the electromagnetic spectrum: current issues in electromagnetic spectrum monitoring," *Electrica*, vol. 18, no. 1, pp. 100–108, 2018.

[4] S. Gurugopinath, R. Akula, C. R. Murthy, R. Prasanna, and B. Amrutur, "Design and implementation of spectrum sensing for cognitive radios with a frequency-hopping primary system," *Physical Communication*, vol. 17, pp. 172–184, 2015.

[5] T. J. Rouphael, *RF and digital signal processing for software-defined radio: a multi-standard multi-mode approach*. Elsevier, 2009.

[6] H. Shin, K. Choi, Y. Park, J. Choi, and Y. Kim, "Security analysis of fhss-type drone controller," in *International Workshop on Information Security Applications*. Springer, 2015, pp. 240–253.

[7] J. H. Gass, P. J. Curry, and C. J. Langford, "An application of turbo trellis-coded modulation to tactical communications," in *MILCOM 1999. IEEE Military Communications. Conference Proceedings (Cat. No. 99CH36341)*, vol. 1. IEEE, 1999, pp. 530–533.

[8] S. Kahveci and T. Atasoy, "From wireless personal area network (wpan) to long range (lora) technology," in *2019 11th International Conference on Electrical and Electronics Engineering (ELECO)*. IEEE, 2019, pp. 679–681.

[9] Rohde & Schwarz GmbH & Co. KG, "Solutions for aviation," *White Paper*, 2019, https://scdn.rohde-schwarz.com/ur/pws/dl_downloads/dl_common_library/dl_brochures_and_datasheets/pdf_1/Aviation_bro_en_3609-3536-42_v0100_120dpi.pdf.

[10] D. D. Coleman and D. A. Westcott, *CWNA: Certified Wireless Network Administrator Official Study Guide: Exam CWNA-106*. John Wiley & Sons, 2014.

[11] X. Liang, Y. Jiang, and T. A. Gulliver, "An improved sensing method using radio frequency detection," *Physical Communication*, vol. 36, p. 100763, 2019.

[12] Y. Li, "Saudi oil production cut by 50% after drones attack crude facilities," *CNBC*, 2019, https://www.cnbc.com/2019/09/14/saudi-arabia-is-shutting-down-half-of-its-oil-production-after-drone-attack-wsj-says.html.

[13] A. Wong, "Singaporeans arrested for smuggling drugs with a drone from malaysia," *Soya Cincau*, 2020, https://www.soyacincau.com/2020/06/21/singaporean-smuggle-drugs-dji-mavic-air-2-drone-jb-kranji/.

[14] B. Boashash, *Time-frequency signal analysis and processing: a comprehensive reference*. Academic press, 2015.

[15] W. Fu, Y. Hei, and X. Li, "Ubss and blind parameters estimation algorithms for synchronous orthogonal fh signals," *Journal of Systems Engineering and Electronics*, vol. 25, no. 6, pp. 911–920, 2014.

[16] A. A. Ahmad and A. Z. Sha'ameri, "Classification of airborne radar signals based on pulse feature estimation using time-frequency analysis," *Defence S&T Tech. Bull*, vol. 8, no. 2, pp. 103–120, 2015.

[17] S. G. Mallat, "A theory for multiresolution signal decomposition: the wavelet representation," in *Fundamental Papers in Wavelet Theory*. Princeton University Press, 2009, pp. 494–513.

[18] A. Z. Sha'ameri, "Analysis and parameter estimation of time-varying signals: theory and methods," in *Journal of Physics: Conference Series*, vol. 1367, no. 1. IOP Publishing, 2019, p. 012091.

[19] F. Hlawatsch and G. F. Boudreaux-Bartels, "Linear and quadratic time-frequency signal representations," *IEEE signal processing magazine*, vol. 9, no. 2, pp. 21–67, 1992.

[20] A. Kanaa and A. Z. Sha'ameri, "A robust parameter estimation of fhss signals using time–frequency analysis in a non-cooperative environment," *Physical Communication*, vol. 26, pp. 9–20, 2018.

[21] B. Ratner, *Statistical and machine-learning data mining:: Techniques for better predictive modeling and analysis of big data*. CRC Press, 2017.

[22] M. P. Gawande and D. G. Agrawal, "Face recognition using pca and different distance classifiers," *IOSR Journal of Electronics and Communication Engineering (IOSR-JECE)*, vol. 9, no. 1, pp. 1–5, 2014.

[23] M. Büchler, S. Allegro, S. Launer, and N. Dillier, "Sound classification in hearing aids inspired by auditory scene analysis," *EURASIP Journal on Advances in Signal Processing*, vol. 2005, no. 18, pp. 2991–3002, 2005.

[24] M. T. Khan, A. Z. Sha'ameri, M. M. A. Zabidi, and C. C. Chia, "Fhss signals classification by linear discriminant in a multi-signal environment," in *Proceedings of the International e-Conference on Intelligent Systems and Signal Processing*. Springer, 2022, pp. 143–155.

[25] J. L. Xu, W. Su, and M. Zhou, "Likelihood-ratio approaches to automatic modulation classification," *IEEE Transactions on Systems, Man, and Cybernetics, Part C (Applications and Reviews)*, vol. 41, no. 4, pp. 455–469, 2010.

[26] M. Azarbad, S. Hakimi, and A. Ebrahimzadeh, "Automatic recognition of digital communication signal," *International journal of energy, information and communications*, vol. 3, no. 4, pp. 21–33, 2012.

[27] P. Kashyap, *Machine learning for decision makers: Cognitive computing fundamentals for better decision making*. Springer, 2017.

[28] V.-T. Tran and W.-H. Tsai, "Stethoscope-sensed speech and breath-sounds for person identification with sparse training data," *IEEE Sensors Journal*, vol. 20, no. 2, pp. 848–859, 2019.

[29] J. Lundén and V. Koivunen, "Automatic radar waveform recognition," *IEEE Journal of Selected Topics in Signal Processing*, vol. 1, no. 1, pp. 124–136, 2007.

[30] G. López-Risueño, J. Grajal, and A. Sanz-Osorio, "Digital channelized receiver based on time-frequency analysis for signal interception," *IEEE Transactions on Aerospace and Electronic Systems*, vol. 41, no. 3, pp. 879–898, 2005.

[31] W. Li, Z. Dou, L. Qi, and C. Shi, "Wavelet transform based modulation classification for 5g and uav communication in multipath fading channel," *Physical Communication*, vol. 34, pp. 272–282, 2019.

[32] M. Zhang, L. Liu, and M. Diao, "Lpi radar waveform recognition based on time-frequency distribution," *Sensors*, vol. 16, no. 10, p. 1682, 2016.

[33] S. M. Abd Elrahman and A. Abraham, "A review of class imbalance problem," *Journal of Network and Innovative Computing*, vol. 1, no. 2013, pp. 332–340, 2013.

[34] J. A. Sáez, B. Krawczyk, and M. Woźniak, "Analyzing the oversampling of different classes and types of examples in multi-class imbalanced datasets," *Pattern Recognition*, vol. 57, pp. 164–178, 2016.

[35] M. A. Mazurowski, P. A. Habas, J. M. Zurada, J. Y. Lo, J. A. Baker, and G. D. Tourassi, "Training neural network classifiers for medical decision making: The effects of imbalanced datasets on classification performance," *Neural networks*, vol. 21, no. 2-3, pp. 427–436, 2008.

[36] U. R. Acharya, S. L. Oh, Y. Hagiwara, J. H. Tan, M. Adam, A. Gertych, and R. San Tan, "A deep convolutional neural network model to classify heartbeats," *Computers in biology and medicine*, vol. 89, pp. 389–396, 2017.

[37] N. Japkowicz and S. Stephen, "The class imbalance problem: A systematic study," *Intelligent data analysis*, vol. 6, no. 5, pp. 429–449, 2002.

[38] N. V. Chawla, K. W. Bowyer, L. O. Hall, and W. P. Kegelmeyer, "Smote: synthetic minority over-sampling technique," *Journal of artificial intelligence research*, vol. 16, pp. 321–357, 2002.

[39] S. Barua, M. M. Islam, X. Yao, and K. Murase, "Mwmote–majority weighted minority oversampling technique for imbalanced data set learning," *IEEE Transactions on knowledge and data engineering*, vol. 26, no. 2, pp. 405–425, 2012.

[40] Rohde & Schwarz GmbH & Co. KG, "Protecting the sky: Signal monitoring of radio controlled civilian unmanned aerial vehicles and possible countermeasures," *White Paper*, 2015, https://www.rohde-schwarz.com/us/campaigns/rsa/gov/protecting-the-sky_231615.html.

[41] F. Liu, M. W. Marcellin, N. A. Goodman, and A. Bilgin, "Compressive sampling for detection of frequency-hopping spread spectrum signals," *IEEE Transactions on Signal Processing*, vol. 64, no. 21, pp. 5513–5524, 2016.

[42] H. Schulze and C. Lüders, *Theory and applications of OFDM and CDMA: Wideband wireless communications*. John Wiley & Sons, 2005.

[43] C. C. Chia and A. Z. Sha'ameri, "Adaptive window size and stepped frequency scan spectrogram analysis for drone signal detection in multi-signal environment," *Defence S&T Tech. Bull*, vol. 13, no. 1, pp. 41–60, 2020.

[44] B. Kaplan, İ. Kahraman, A. Görçin, H. A. Çırpan, and A. R. Ekti, "Measurement based fhss–type drone controller detection at 2.4 ghz: An stft approach," in *2020 IEEE 91st Vehicular Technology Conference (VTC2020-Spring)*. IEEE, 2020, pp. 1–6.

[45] P. Kadam and S. Bhalerao, "Sample size calculation," *International journal of Ayurveda research*, vol. 1, no. 1, p. 55, 2010.

[46] R. V. Krejcie and D. W. Morgan, "Determining sample size for research activities," *Educational and psychological measurement*, vol. 30, no. 3, pp. 607–610, 1970.

[47] H. Xiao, Y. Q. Shi, W. Su, and J. A. Kosinski, "Automatic classification of analog modulation schemes," in *2012 IEEE Radio and Wireless Symposium*. IEEE, 2012, pp. 5–8.

[48] C. M. Bishop, *Neural networks for pattern recognition*. Oxford university press, 1995.

[49] M. F. Møller, "A scaled conjugate gradient algorithm for fast supervised learning," *Neural networks*, vol. 6, no. 4, pp. 525–533, 1993.

[50] M. S. B. H. Salam, D. Mohamad, and S. H. S. Salleh, "Temporal speech normalization methods comparison in speech recognition using neural network," in *2009 International Conference of Soft Computing and Pattern Recognition*. IEEE, 2009, pp. 442–447.

[51] J. D. Rodriguez, A. Perez, and J. A. Lozano, "Sensitivity analysis of k-fold cross validation in prediction error estimation," *IEEE Transactions on Pattern Analysis and Machine Intelligence*, vol. 32, no. 3, pp. 569–575, 2009.

[52] H. Wickham and L. Stryjewski, "40 years of boxplots," 2011, http://vita.had.co.nz/papers/boxplots.pdf.

[53] M. A. Nielsen, *Neural networks and deep learning*. Determination Press, 2015, vol. 25.

[54] L. Prechelt, "Early stopping-but when?" in *Neural Networks: Tricks of the trade*. Springer, 1998, pp. 55–69.

Muhammad Turyalai Khan received his B.Sc. in Computer Engineering from the COMSATS university, Islamabad, Pakistan in 2012 and M.S. in Electrical Engineering from the RIU, Islamabad, Pakistan in 2015. Currently, he is pursuing his Ph.D. in Electrical Engineering from the UTM, Malaysia. His research interests include machine learning, data science, and digital signal and image processing

Ahmad Zuri Sha'ameri received his M.Eng. in Electrical Engineering and Ph.D. both from the UTM, Malaysia in 1991 and 2000 respectively. Currently, he is the Head of the DSP Lab, Faculty of Electrical Engineering, UTM. His research interests include signal theory, signal analysis and classification, and information security.

Muhammad Mun'im Ahmad Zabidi received his M.S. in Computer Engineering from the University of Bridgeport, USA in 1988. He is currently a Senior Lecturer at the UTM, Malaysia. His research interests include artificial intelligence, bioacoustics, and embedded systems.